

Ultraviolet Mg II emission from fast neutral ejecta around Eta Carinae

Nathan Smith^{1*} and Jon A. Morse²

¹*Steward Observatory, University of Arizona, 933 N. Cherry Ave., Tucson, AZ 85721, USA*

²*BoldlyGo Institute, 1370 Broadway 5th Floor Suite 572, New York, NY 10018, USA*

19 July 2019

ABSTRACT

We present the first images of the nebula around η Carinae obtained with the Wide Field Camera 3 (WFC3) onboard the *Hubble Space Telescope* (*HST*), including an ultraviolet (UV) image in the F280N filter that traces Mg II emission, plus contemporaneous imaging in the F336W, F658N, and F126N filters that trace near-UV continuum, [N II], and [Fe II], respectively. The F336W and F658N images are consistent with previous images in these filters, and F126N shows that for the most part, [Fe II] λ 12567 traces clumpy shocked gas seen in [N II]. The F280N image, however, reveals Mg II emission from structures that have not been seen in any previous line or continuum images of η Carinae. This image shows diffuse Mg II emission immediately outside the bipolar Homunculus nebula in all directions, but with the strongest emission concentrated over the poles. The diffuse structure with prominent radial streaks, plus an anticorrelation with ionized tracers of clumpy shocked gas, leads us to suggest that this is primarily Mg II resonant scattering from unshocked, neutral atomic gas. We discuss the implied structure and geometry of the Mg II emission, and its relation to the Homunculus lobes and various other complex nebular structures. An order of magnitude estimate of the neutral gas mass traced by Mg II is $0.02 M_{\odot}$, with a corresponding kinetic energy around 10^{47} erg. This may provide important constraints on polar mass loss in the early phases of the Great Eruption. We argue that the Mg II line may be an excellent tracer of significant reservoirs of freely expanding, unshocked, and otherwise invisible neutral atomic gas in a variety of stellar outflows.

Key words: circumstellar matter — stars: evolution — stars: winds, outflows

1 INTRODUCTION

The massive evolved star η Carinae is surrounded by a beautifully complex system of nebulosity that seems to get more complicated and interesting the closer we look. The main components in images are the prominent bipolar nebula known as the “Homunculus” (Gaviola 1950), which is mostly a dusty reflection nebula, as well as the more extended ragged splash of ionized condensations known as the “Outer Ejecta” (Walborn 1976). The Outer Ejecta are accompanied by a large shell seen in soft X-rays (Seward et al. 2001), indicating that fast ejecta are overtaking and shocking older, slower material from previous mass loss. The Outer Ejecta are N-rich (Walborn 1976; Davidson et al. 1982), while the degree of N enrichment is greater inside the X-ray shell than outside of it (Smith & Morse 2004). These nebular features represent the combined mass loss of a few energetic, eruptive mass loss events over the past several hundred years, includ-

ing the “Great Eruption” in the mid-19th century and earlier undocumented events (Morse et al. 2001; Kiminki et al. 2016; Smith 2017). Although poorly understood, episodic mass loss may play an important role in stellar evolution (Smith & Owocki 2006; Smith 2014), at least for a subset of stars in interacting binaries (Smith & Tombleson 2015; Aghakhanloo et al. 2017).

The eruption of η Car and its resulting nebula are uniquely valuable for studying episodic mass loss from massive stars because we have the historical visual magnitudes of the 19th century outburst (Herschel 1847; Smith & Frew 2011), along with light-echo spectroscopy of reflected light from the event (Rest et al. 2012; Prieto et al. 2014; Smith et al. 2018a,b), both of which can be compared to contemporary extragalactic analogs of LBV eruptions (Van Dyk & Matheson 2012; Smith et al. 2011). Unlike extragalactic LBV eruptions, we can also dissect the structural details of the remnant ejecta nebula that is the mass-loss product of that previous event, and we can study the current post-eruption state of the surviving star.

* E-mail: nathans@as.arizona.edu

While the mass loss in the 19th century eruption has traditionally been discussed as the result of a clumpy super-Eddington radiation-driven wind (Shaviv 2000; Owocki et al. 2004; van Marle et al. 2008, 2009), some clues have hinted that an explosive mechanism may have been important. These clues include a high ratio of kinetic to radiated energy (Smith et al. 2003b), the very thin walls and double-shell structure of the Homunculus lobes (Smith 2006, 2013), and some very high observed velocities in the outer ejecta (Smith 2008). Smith (2013) outlined how the nebula and historical light curve could be reconciled with a model where the light curve was powered by the shock interaction between fast explosive ejecta and slower circumstellar material (CSM interaction), analogous to a scaled-down version of a Type II_n supernova (SN). More recently, spectroscopy of light echoes from η Car’s eruption provide strong confirming evidence of a shock-powered event (Smith et al. 2018a,b), revealing extremely high speed ejecta expanding at around 10,000 km s⁻¹ or more, seen simultaneously with slower ejecta around 150 and 600 km s⁻¹, and a time sequence of echo spectra that closely mimics the spectral evolution seen in Type II_n SNe powered by CSM interaction.

These recent data imply that the current nebulosity around η Car may closely resemble a low-energy supernova remnant (SNR). Obviously the nature of the explosive event was different, since core-collapse SNe are terminal explosions, whereas η Car’s 19th century eruption was an incomplete, non-terminal explosion that left behind a surviving very massive star. Nevertheless, the current X-ray shell is quite similar to an SNR in some ways (Seward et al. 2001), and the highly clumped, N-rich outer ejecta can be understood as post-shock cooling features, analogous to shocked CSM material like the N-rich quasi-stationary flocculi in Cas A (Chevalier & Kirshner 1978; Chevalier & Liang 1989). Walborn (1976) pointed out the similarity between η Car’s Outer Ejecta and these features in Cas A many years ago. Interestingly, the physical parameters of η Car’s eruption also provide a surprisingly good match to predictions of multiple massive shell collisions that occur in exotic events such as pulsational pair instability SNe (Woosley 2017). Compared to traditional core-collapse SNe, non-terminal explosions are, however, relatively unexplored and far less well understood; detailed analysis of the structure, kinematics, and excitation of nebulosity resulting from such an event may be quite valuable for constraining future models.

The *Hubble Space Telescope* (*HST*) has had a tremendous impact on our understanding of η Carinae and its nebula. The first *HST* images of η Carinae with WF/PC (Hester et al. 1991), WFPC2 (Morse et al. 1998), and ACS/HRC (Smith et al. 2004a) each revealed new, complex, and sometimes mysterious structural details in the nebula.¹ Multi-epoch images with *HST* also reveal detailed photometric variability on small spatial scales in the nebula (Smith et al. 2000, 2004b; Smith 2017), as reflected starlight

and line emission respond to variations of the star during its 5.5 yr orbital cycle (Damineli 1996) and long-term changes. The unprecedented angular resolution of *HST* has also enabled high-precision proper-motion measurements for the expanding Homunculus and other ejecta close to the star (Currie et al. 1996; Morse et al. 2001; Dorland et al. 2004; Smith et al. 2004a; Weigelt & Kraus 2012; Smith 2017). The most recent results, with a baseline over nearly the entire post-COSTAR lifetime of *HST*, yield a precise dynamical date of origin for the Homunculus of 1847.1 ± 0.8 yr (Smith 2017), while some features close to the star and inside the Homunculus are younger (Dorland et al. 2004; Smith et al. 2004a). Similarly, *HST* images have been used to measure the proper motions of the Outer Ejecta (Morse et al. 2001; Kiminki et al. 2016), revealing a mix of dynamical ages that indicate previous mass-loss episodes centuries before the Great Eruption. Overall, these *HST* images largely trace starlight scattered by dust in the Homunculus (with some contribution from line emission in various features), and line emission from shock-ionized gas in the Outer Ejecta.

Additionally, both ground-based and *HST* spectra have provided radial velocities that, when combined with structures in images, helped to decipher the 3-D structure and kinematics of the Homunculus and Outer Ejecta (Hillier & Allen 1992; Weis et al. 1999, 2001; Weis 2012; Davidson et al. 2001; Currie et al. 2002; Ishibashi et al. 2003; Smith 2002a, 2004, 2005, 2006, 2008; Smith et al. 2003a; Teodoro et al. 2008; Weigelt & Kraus 2012; Steffen et al. 2014; Mehner et al. 2016). High angular resolution mid-infrared (mid-IR) and submm images have traced thermal emission from warm dust in the thin Homunculus lobes and equatorial region (Chesneau et al. 2005; Smith et al. 2003b, 2018c), while near-IR line emission from H₂ (Smith & Davidson 2001; Smith 2002a, 2004, 2006; Smith & Ferland 2007; Steffen et al. 2014) and UV absorption in the line of sight through the SE polar lobe (Gull et al. 2005, 2006; Nielsen et al. 2005; Verner et al. 2005) have probed the thin molecular shell and dense atomic gas in the Homunculus walls.

A rarely noted feature that is directly relevant to the discussion here is a polar bubble or shell immediately outside the Homunculus south-east (SE) lobe seen in Ca II HK absorption and He I λ 10830 absorption (Smith 2002a; Davidson et al. 2001), and in emission lines like H α and [N II] λ 6584 (Currie et al. 2002; Smith et al. 2003a; Mehner et al. 2016), and near-IR [Fe II] (Smith 2002a). There may be a corresponding bubble over the NW polar lobe (Mehner et al. 2016), but it cannot be seen in absorption. Currie et al. (2002) referred to the SE polar bubble as the “ghost shell”, although it may be a more complex structure as discussed below. It appears related to – but is not the same as – features seen in our new Mg II image.

Here we present the first UV images of η Car in the light of emission from the Mg II λ 2796, 2803 resonant doublet taken through the F280N filter with the *HST* Wide Field Camera 3 (WFC3). UV imaging at similar wavelengths in broad continuum filters (F220W and F250W) obtained with the ACS High Resolution Channel (HRC) was reported previously (Smith et al. 2004a,b), but had shorter exposures only tracing the bright Homunculus, dominated by dust-scattered starlight plus some diffuse line emission that creates a “Purple Haze” close to the star. The new Mg II images

¹ Note that in this discussion we are referring to previous work on the extended nebula around η Car. In the interest of brevity, we do not refer to the vast literature concerning the central star, its immediate vicinity, its binary-induced multi-wavelength variability, or its colliding stellar winds.

Table 1. WFC3 UVIS and IR Channel Observation Log^a

UT Date (2018)	Filter	$\lambda_{peak}/$ Width (Å)	Diagnostic (Ejecta)	Total Exposure
05 Mar	F280N	2798/43	Mg II	7860s
06 Mar	F126N	12590/152	[Fe II]	1997s
25 Jul	F280N	2798/43	Mg II	6, 40 s
25 Jul	F336W	3375/511	NUV, [N II]	1, 16, 240s
25 Jul	F658N	6585/28	[N II]	1, 16, 540s

^a Programs GO-15289 and GO-15596.

presented here are deeper, and the UV line emission reveals structures not traced by any previous diagnostic. Section 2 presents the new *HST*/WFC3 observations, Section 3 briefly lists the main results of the imaging, and Section 4 includes an interpretation of various features, an analysis of the Mg II emission, and discusses the structure of the Homunculus and Outer Ejecta in context with several other multi-wavelength diagnostics from the literature.

2 OBSERVATIONS

η Car was observed through the UVIS and IR channels of WFC3 in two observing epochs. The initial observations (*HST* program ID 15289) occurred in March 2018 through the UVIS F280N (Mg II) filter and IR F126N ([Fe II]) and F130N (IR continuum) filters.

We used the standard STSDAS pipeline image reduction process for all images, which performed bias-subtraction, flat-fielding, removal of cosmic rays, geometric distortion correction and flux calibration. Small offsets/dithers were used during the observations to recognize and correct for bad pixels on the UVIS CCD detectors and to limit the number and bleeding of saturated CCD pixels caused by the bright central star. Ultimately, twelve 655 sec F280N exposures, for a total exposure time of 7860 secs, were combined by the DRIZZLE task into a single Mg II image. This deep image was captured to trace emission from the fast-moving ejecta outside of the Homunculus; however, as a result the inner ~ 1 arcsecond around the central star was saturated in the final processed image.

The IR channel observations were programmed to avoid placing the central star on the detector. Using different roll angles and spatial offsets, the central star was moved sequentially off the edges of the square detector so that the rims of the Homunculus lobes and outer ejecta could be observed. Unfortunately, two of the four orientations appear to have experienced guiding problems, so that F126N and F130N mosaics of the entire region around the Homunculus were not possible. In this study, we focus on the F126N ([Fe II]) image in the orientation that captured the rim of the SE lobe, S Ridge and E Condensations, using the terminology of [Walborn et al. \(1978\)](#), and compare this to the emission observed through other filters.

The purpose of comparing the UV Mg II and near-IR [Fe II] is that these ions trace similar temperatures in post-shock gaseous structures. These lines appear in radiative shock models ([Hartigan et al. 1987, 2004](#)), along with other common visible emission lines (H α , [N II], [S II], etc.) from different temperature regimes, and may be compared to indicate local density, extinction and/or abundance variations.

Also, the near-UV imaging offers the highest spatial resolution full-field WFC3 emission-line imaging.

As discussed in more detail in Sec. 3, there is significant overlap between the Mg II and [N II] emission, particularly in bright [N II] outer ejecta knots such as the S Condensation. However, those are not the brightest features in the Mg II image, which instead reveals a host of hitherto unseen filaments and structures related to both bipolar and equatorial structures. The Mg II emission largely complements – that is, lies adjacent to, often along contiguous structures – the [N II] emission. This intriguing relationship was evident even when comparing the new F280N image with *HST* WFPC2 F658N images from the 1990s, despite arcsecond-scale proper motions of the bipolar lobes and outer debris. In order to make detailed comparisons at the scale of small knots and filaments, we therefore requested and were approved for 1 orbit of Director’s Discretionary Time (program ID 15596) to obtain contemporaneous WFC3 [N II] (F658N) and blue continuum (F336W) observations, which were filters used in past imaging *HST* imaging campaigns. We also acquired short duration Mg II (F280N) images to mitigate the saturated pixels near the central star in the original program.

Sequences of images with different exposure times were obtained in July 2018 through the F280N, F336W and F658N filters in order to cover the large dynamic range between the η Car central star and faint filaments in the outer debris (see Table 1). In order to fit the exposure sequences into a single WFC3 buffer dump to the *HST* solid state recorder, we used 1024×1024 subarrays for the short and medium exposures – since we were only interested in the pixels around the central star – and then 2048×2048 subarrays for the longest F336W and F658N exposures. Saturated pixels near the central star and associated bleeding in longer exposures were masked out, and pixel flux values from shorter exposure images were scaled and substituted. Even though the 2048×2048 subarray used for the long exposures was only a quarter of the full WFC3 field of view, the images covered most of the important Outer Ejecta and, at 40 milli-arcseconds per pixel, had essentially the same field of view as previous WFPC2 WF camera images (approximately 800×800 at ~ 100 milli-arcseconds per pixel) but with better than PC resolution. Finally, we deconvolved each image conservatively for 3 iterations using the Lucy-Richardson algorithm provided in STSDAS. The images were rotated and aligned to our historical dataset of WFPC2 images using IRAF² tasks and about seven stars common to all images as tie points.

Table 1 summarizes the observations used in this study, indicating the filters, exposure times, and principal contributors to the observed features. We note that every image through all the filters contains some sort of internal reflection ghost and/or scattered light from the bright central star, which vary as a function of *HST* roll angle and where the central star was placed in the field of view. Such artifacts

² IRAF is distributed by the National Optical Astronomy Observatories, which is operated by the Association of Universities for Research in Astronomy, Inc. (AURA) under cooperative agreement with the National Science Foundation. The Space Telescope Science Data Analysis System (STSDAS) is distributed by the Space Telescope Science Institute.

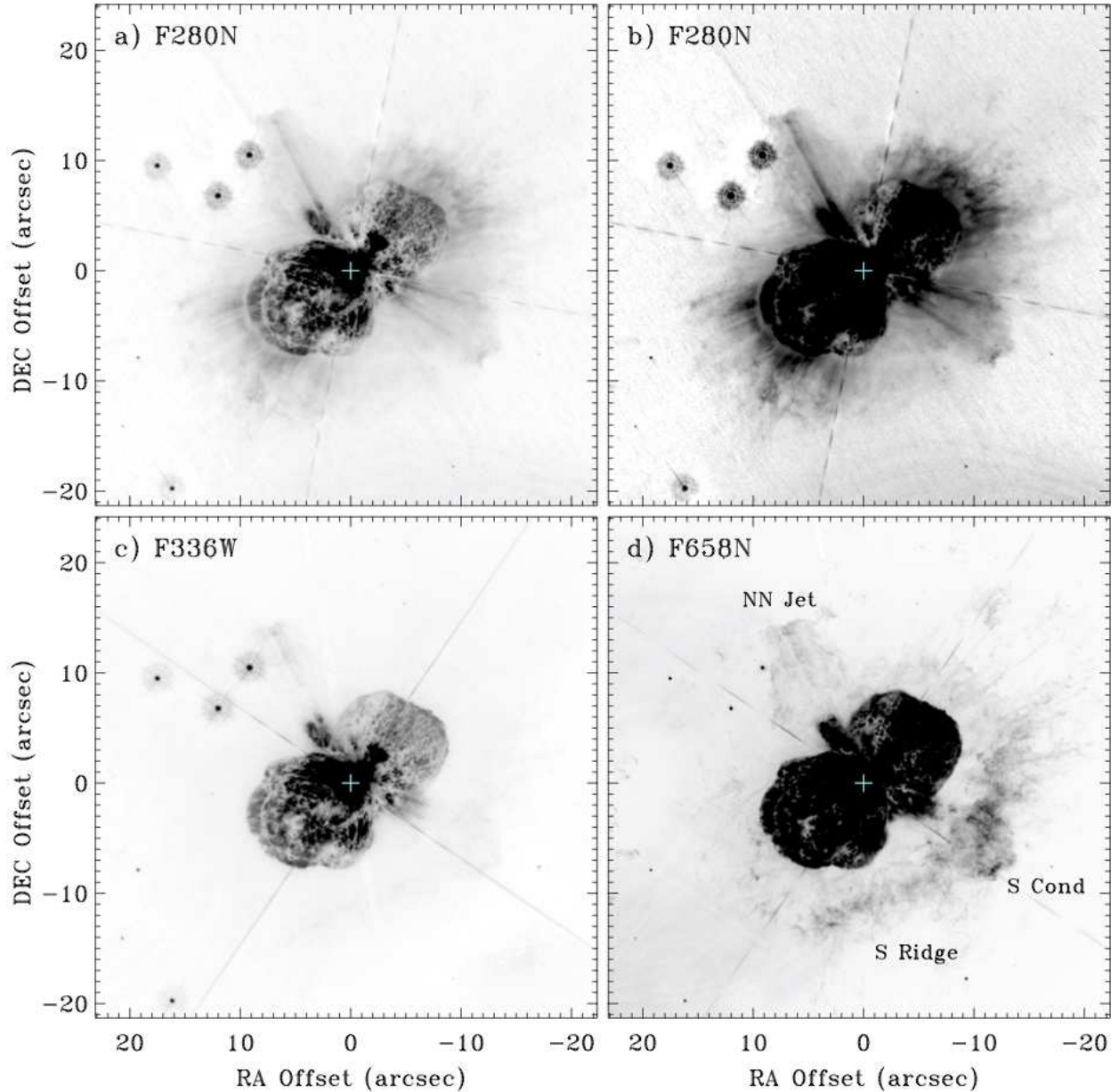


Figure 1. Comparison of new deconvolved near-UV *HST*/WFC3 images of η Car in the F280N Mg II filter (a,b), the F336W near-UV continuum filter (c), and the F658N [N II] λ 6584 filter (d). Panels *a* and *b* show the same F280N image with two different intensity stretches, with Panel *a* scaled to show brighter features for comparison with the F336W continuum image, and with Panel *b* scaled to show the faintest detected Mg II emission.

limit how faint we can see in certain regions, and we therefore focus on the Homunculus and brighter Outer Ejecta emission-line features. We also note detectable fractional-pixel proper motions of the fast-moving debris between the March 2018 exposures through the F280N filter and those from July 2018 through F336W and F658N. The motions are barely discernible when blinking the images in an image display, but we nonetheless avoid over-interpreting very small-scale differences until we can obtain images within the same day or week in a future campaign.

It is also important to keep in mind, particularly for the narrowband filters, the limited and varying velocity ranges that are recorded in the images. The F658N filter has the

narrowest width (see Table 1), covering a velocity range in [N II] λ 6583 emission of about ± 650 km s $^{-1}$, plus redshifted H α emission from about +350 to +1600 km s $^{-1}$. The F280N filter covers a larger velocity range in Mg II emission of about ± 2300 km s $^{-1}$, while the near-IR F126N filter covers ± 1800 km s $^{-1}$ in [Fe II]. Given these velocity range differences, it is possible that there is some missing emission when comparing the morphologies in the different diagnostic features. Nevertheless, given the similarities between the [Fe II] and [N II] emission features, and how distinct the Mg II features between the Homunculus lobes and outer, [N II]-bright ejecta generally are (see discussion below), we believe that the observed emission represents real distributions of the neutral

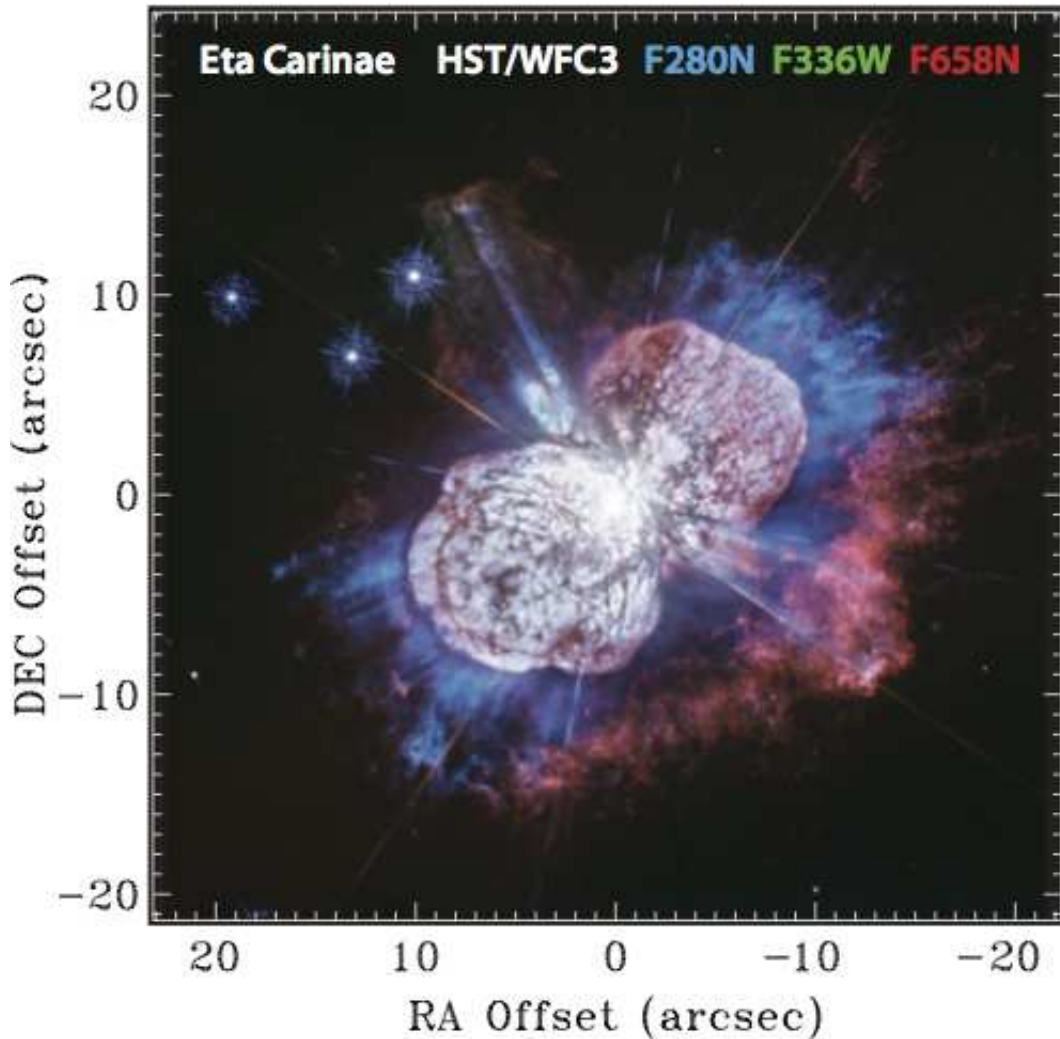


Figure 2. Color *HST*/WFC3 image of η Car with F280N in blue, F336W in green, and F658N in red.

and ionized gas, and are not artifacts of the different filter widths. Future proper-motion and spectroscopic observations could definitively verify this.

3 RESULTS

Various features in the new WFC3 images are discussed in the following subsections. Figure 1 shows the deconvolved WFC3-UVIS images in the F280N (two intensity ranges), F336W, and F658N filters. Figure 2 presents a 3-color composite of these same images with F280N in blue, F336W in green, and F658N in red. Figure 3 shows the portion of the Outer Ejecta imaged in [Fe II] emission in the F126N filter of WFC3-IR, as well as aligned portions of the same three WFC3-UVIS images as in previous figures. Figure 4 shows intensity scans crossing the Homunculus at several positions parallel to the polar axis in the F280N (blue), F336W (gray), and F658N (orange) filters. Figure 5 shows images representing the intensity ratio of F280N/F336W and F280N/F658N, highlighting the differences between Mg II emission and the other lines. Finally, Figure 6 illustrates the spatial relationship between the 0.5-7 keV X-ray emission from the Outer

Ejecta seen by *Chandra*, shown in purple, and the same 3-color WFC3-UVIS image from Figure 2.

3.1 F280N Mg II Emission

In the F280N filter, the main part of the bipolar Homunculus nebula is dominated by near-UV dust-scattered starlight, just as it is in most broad band UV/optical filters, and very similar to the near-UV scattered continuum in the F336W filter (compare Figures 1a and 1c). However, F280N also reveals Mg II emission structures immediately outside the Homunculus that are either absent or far less pronounced at any other wavelength range that we are aware of (Figure 1; compare panels *a* & *b* to *c* & *d*). Previous UV spectra confirm that Mg II emission dominates the flux in the F280N filter at locations in the Outer Ejecta near the S Condensation (Davidson et al. 1982; Dufour et al. 1999).

In general, the brightest F280N emission outside the Homunculus appears anticorrelated with [N II] emission in the F658N filter. This is best appreciated in the color image in Figure 2 where F280N emission (blue) dominates at most locations immediately outside the main polar lobes of the Homunculus, whereas F658N emission (red) is stronger in

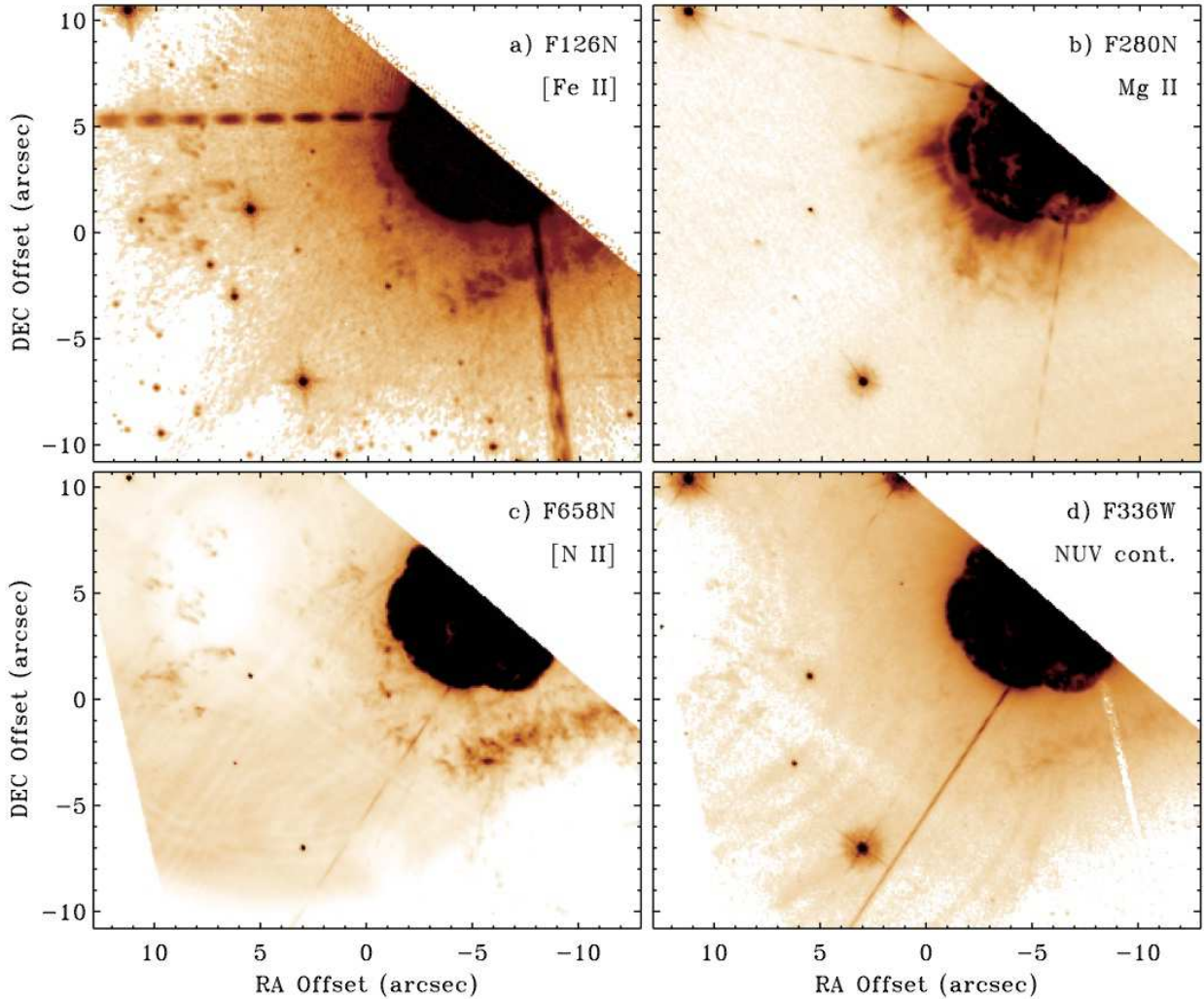


Figure 3. Images aligned to the [Fe II] F126N image, which covered only part of the region around η Car in order to avoid the extremely bright central star. (a) The F126N image, sampling [Fe II] λ 12567, (b) the F280N image, (c) the F658N image including [N II] λ 6584 and some redshifted H α , and (d) the F336W image, which includes mostly near-UV continuum, but includes some line emission from [N I] λ 3466 and various fainter Fe II lines. The bright background in F658N and F336W is due to ghost images of the central star. Positional offsets in arcsec are from an arbitrary point at the center of the image.

a shell at larger separation from the star. Figure 2 gives the impression that Mg II emission fills the cavity inside the [N II]-emitting shell. While a subset of the features seen in F280N can also be seen in F336W and/or F658N, the morphology and intensity distribution is different between these filters, and many structures are only seen in one filter.

Spatial intensity scans of F280N, F336W, and F658N flux are shown in Figure 4, showing that the strength of Mg II emission immediately outside the Homunculus is almost as bright as the scattered near-UV continuum of the polar lobes, whereas the F336W and F658N flux drops precipitously at the outer boundary of the polar lobes. F658N (in some directions) brightens at larger separation, whereas the F280N flux tends to decline smoothly with increasing separation from the star.

Ratio images of F280N/F336W and F280N/F658N are shown in Figures 5a and 5b, respectively. These highlight structures that are particularly enhanced in Mg II line emission but not in other tracers, because they divide out the

near-UV or red continuum scattered light, as well as the H α and [N II] line emission. While Mg II emission is seen from a blue halo encircling the Homunculus in Figure 2, it is also evident from Figure 5 that the Mg II emission is most pronounced over the poles.

Strong Mg II emission, combined with a lack of H α or [N II], indicates that the F280N filter in regions immediately outside the Homunculus (blue in Fig.2, black in Fig.5) is tracing predominantly neutral atomic gas (i.e., neutral H, but low-ionization metals), because Mg⁰ is ionized to Mg⁺ at 7.6 eV, whereas Mg⁺ is ionized at 15 eV. Below in Section 4.1 we discuss why we favor an interpretation of resonant scattering for the Mg II line production rather than post-shock cooling emission. Furthermore, as previously noted, given that the Mg II emission generally lies spatially between the Homunculus lobes and outer ejecta bright in [N II] – such as the S Condensation – we do not believe that the larger velocity range transmitted through the F280N filter is responsible for the morphological differences, and indeed indicates that

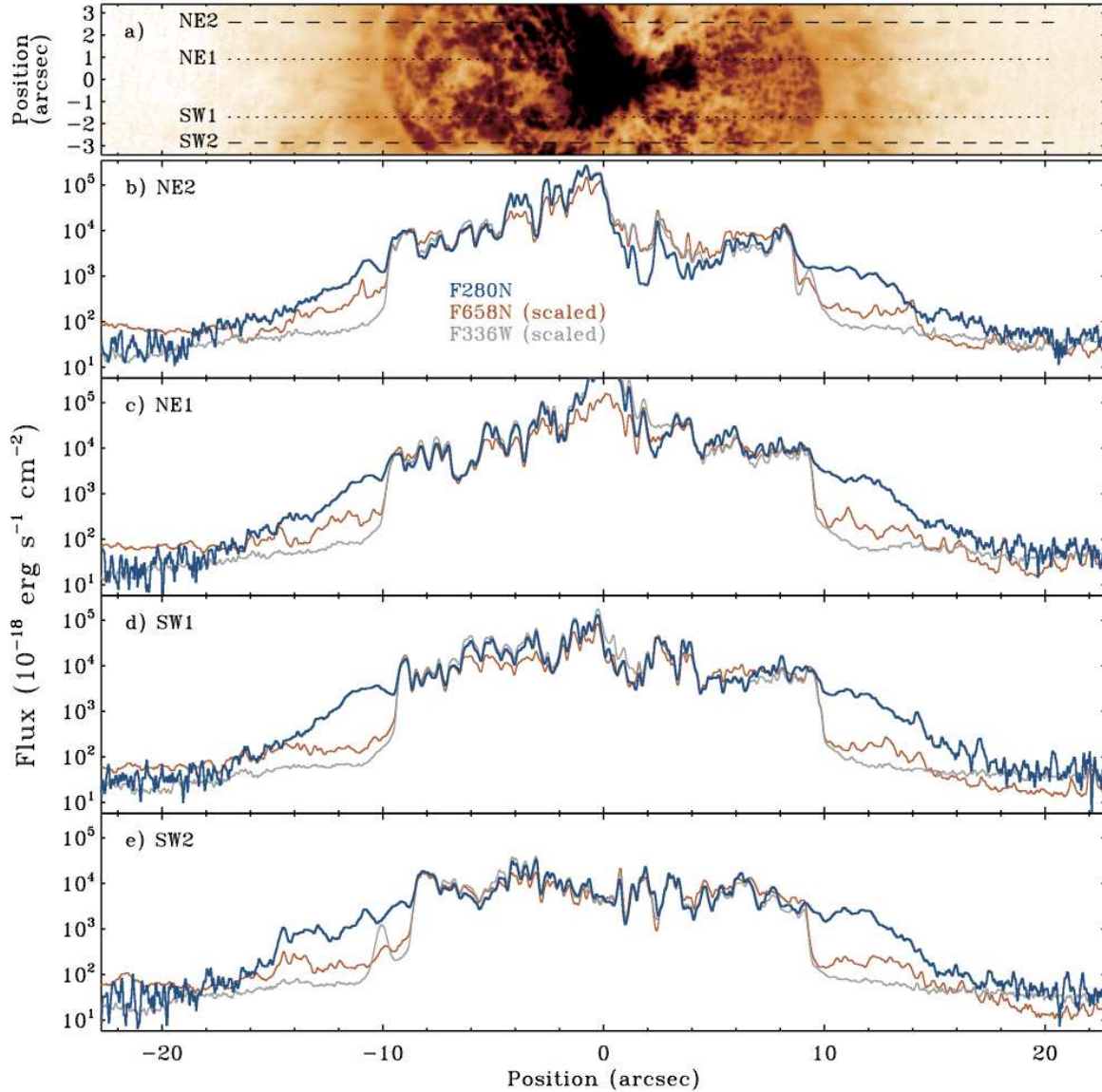


Figure 4. Intensity scans across the Homunculus in WFC3/UVIS images. Top panel (a) shows a portion of the F280N image of the Homunculus, rotated clockwise by 40° so that the polar axis is horizontal. Positions of four scans across the nebula are indicated (northeast 1 and 2, southwest 1 and 2). Panels b (northeast 2), c (northeast 1), d (southwest 1), and e (southwest 2) show intensity scans along the positions indicated in panel a. Each of these scans averaged the flux across 3 spatial pixels, or $0''.07$. Blue is the line flux in the F280N filter. Orange and grey show scaled intensities of F658N and F336W, respectively, where their relative intensity has been adjusted roughly to match the F280N flux of the polar lobes of the Homunculus for comparison.

the Mg II emission (neutral gas) may be confined to lower velocities than the ionized features seen in [N II].

3.2 F336W and F658N

New images in the F336W and F658N filters (Figs. 1c and 1d) show qualitatively the same structure as seen in previous epochs of imaging, as described already by Morse et al. (1998) and other authors. We do not analyze these images further, except to compare them with new images in the F280N and F126N filters. For a detailed comparison with F280N emission, new images in these filters were needed because of the rapid expansion of the nebula.

The flux detected in the broad F336W filter is dominated by near-UV starlight scattered by dust grains in the Homunculus, but there is also a minor contribution from emission lines of low-ionization metals. In the Outer Ejecta, there is no strong contribution from high ionization lines like Ne III or Ne V as in some supernova remnants (Sutherland & Dopita 1995; Blair et al. 2000). Referring to the archival *HST* FOS UV spectrum of the S Condensation (see Dufour et al. 1999), the strongest emission line in the F336W bandpass is [N I] $\lambda 3466$. Such emission is not surprising given the N-rich abundances in the Outer Ejecta, and the wide range of ionization (Davidson et al. 1982; Smith & Morse 2004). This [N I] emission is faint, and it appears to track the [Fe II] and [N II] emission (see below).

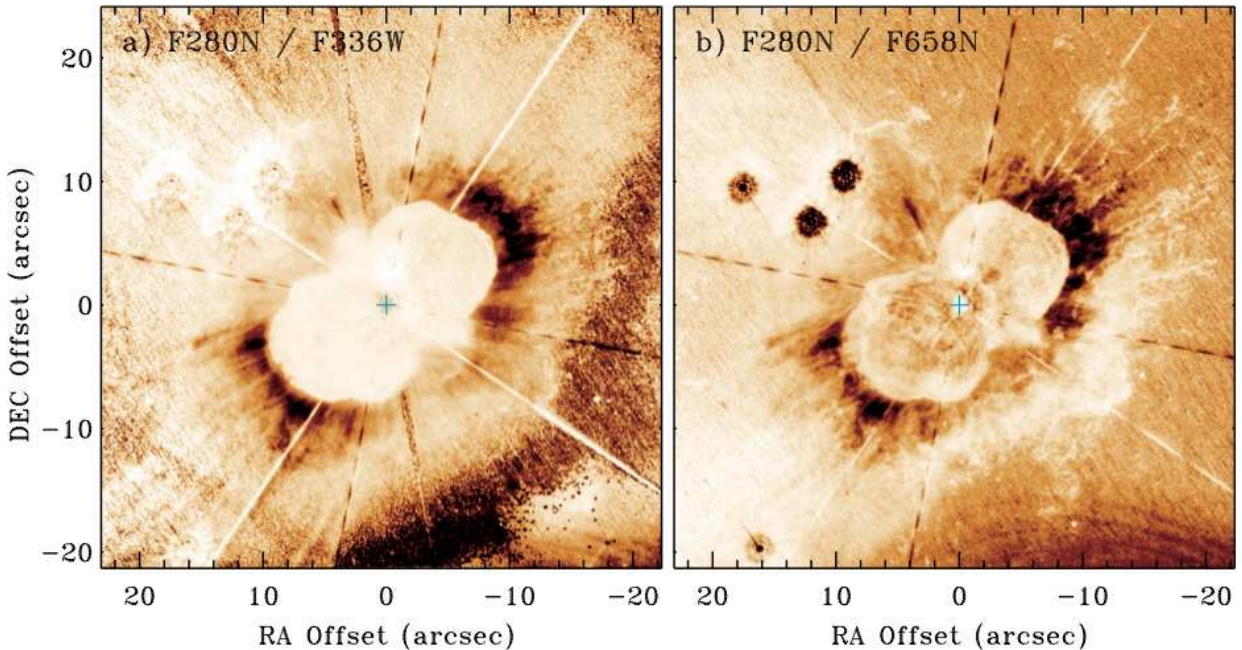


Figure 5. Ratio images. (a) Relative flux ratio of F280N / F336W. Features that are relatively bright in F280N are dark, and the near UV continuum or [N I] emission is light. (b) Ratio image of F280N / F658N, where regions with relatively strong Mg II emission are dark, and locations of strong [N II] emission are light. The lighter regions of diffuse background at the left portions of each panel are due mostly to excess flux from ghost images of the bright central star in the F336W and F658N images.

The narrow F658N filter is also dominated by scattered continuum starlight in the bipolar lobes of the Homunculus (or perhaps more accurately, a combination of scattered continuum plus dust-scattered and redshifted $H\alpha$ from the central star’s wind; see [Smith et al. 2003a](#)), but is primarily tracing intrinsic [N II] $\lambda 6584$ emission and a small amount of redshifted $H\alpha$ recombination emission in the Outer Ejecta. In the Outer Ejecta, this emission traces gas that has been collisionally excited and ionized by a shock, which is rapidly cooling and fragmenting. This is why the F658N image of the Outer Ejecta has a morphology consisting of a complex arrangement of strings, clumps, shells, filaments, etc. ([Morse et al. 1998](#); [Smith & Morse 2004](#); [Weis et al. 1999, 2001](#)).

3.3 F126N [Fe II] Emission

Near-IR emission from [Fe II] (especially the pair of strong lines at 12567 and 16435 Å) is seen from the shell nebulae around several LBVs, including η Carinae, P Cygni, and others ([Hillier & Allen 1992](#); [Smith 2002a,b](#); [Smith & Hartigan 2006](#)). These lines are thought to be strong in LBVs because the shells are composed of dense, low-ionization gas ([Smith 2002b](#); [Smith & Hartigan 2006](#)). LBVs are strong sources of non-ionizing Balmer continuum UV radiation, but their dense winds can absorb much of the Lyman continuum flux.

Figure 3 shows a WFC3/IR-channel image in the near-IR F126N filter, which samples [Fe II] $\lambda 12567$. The field of view is offset to the SE from the star to avoid the bright central star and the core of the Homunculus; even the SE lobe is saturated in this image. Three other pointings (to the NE, NW, and SW of the star) were planned, but the resulting exposures suffered from tracking problems and other

issues that compromised the quality of the images (as noted above in Section 2).

Figure 3 also shows images aligned to this F126N image in three other filters: F280N (Mg II), F658N ($H\alpha$ and [N II] $\lambda 6583$), and F336W (near-UV continuum plus some weaker emission from [N I] $\lambda 3468$ and several Fe II lines). From this comparison, it seems clear that the [Fe II] line emission is tracing mostly the same gas that glows brightly in the [N II] line in F658N. The E condensations and the dense knots that compose the S Ridge are seen clearly in both F126N and F658N. Since the N-rich knots in these Outer Ejecta exhibit a wide range of ionization in lines from [N I] to N V ([Davidson et al. 1982](#)), they are tracing dense condensations that are rapidly cooling after being ionized by a shock.

On the other hand, the emission in the F280N filter is tracing very different emitting structures from the F658N and F126N filters. Although some of the F280N emission outside the SE lobe overlaps with features seen in F658N, these emitting structures have a very different morphology and radial extent. The F280N emission arises from an entirely different set of gaseous structures, or perhaps a combination of these different structures and some emission from the same knots seen in F658N and F126N. (Spectra of the Mg II line are needed to determine if the radial velocities are distinct from the velocities of [N II] and [Fe II] emission.) Whereas the F658N and F126N filters trace a series of dense clumps that are separated from the Homunculus, the F280N emission is more diffuse, and often exhibits radial streaks immediately outside the polar lobes of the Homunculus. The F280N structures are therefore both morphologically and spatially distinct from the shocked [N II] and [Fe II] clumps. This is one of the main reasons we favor the interpretation that the emission in the F280N filter is resonant scattering

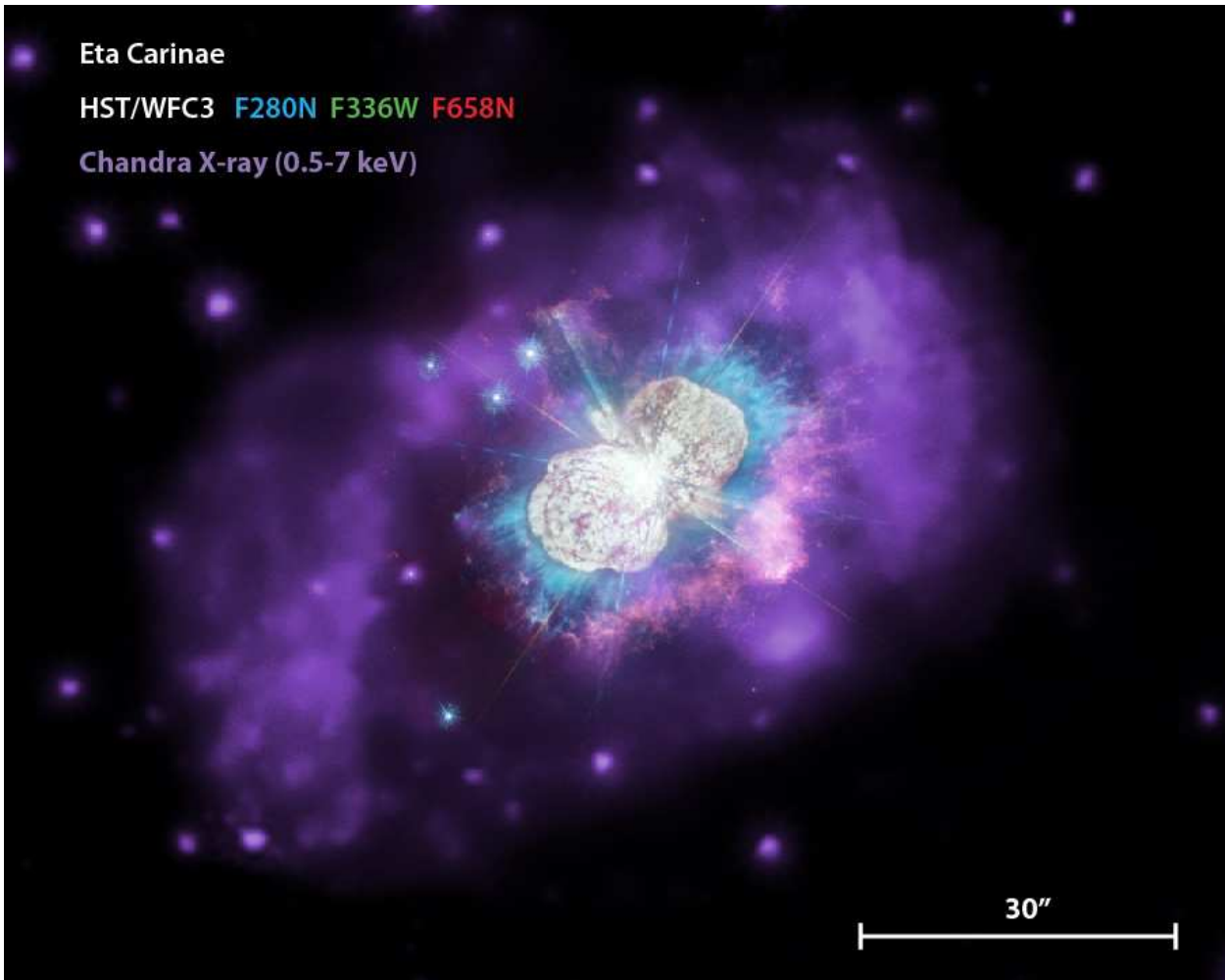


Figure 6. The adaptively smoothed 0.5-7 keV X-ray image of the Outer Ejecta as seen by *Chandra* ACIS-S is shown in purple. Processing and analysis of similar *Chandra* imaging of η Car’s Outer Ejecta have been discussed in detail previously (Seward et al. 2001; Corcoran et al. 2004; Hamaguchi et al. 2014). The 3-color WFC3/UVIS image from Figure 2 is superposed.

of Mg II from freely expanding, low-ionization, unshocked ejecta outside the Homunculus (see below).

4 DISCUSSION

4.1 Mg II Resonant Scattering

We propose that the bulk of the Mg II emission detected in the F280N filter that is seen outside the Homunculus but inside the N-rich shell of Outer Ejecta arises predominantly from resonant scattering in the Mg II $\lambda\lambda 2796, 2803$ doublet. Resonant scattering traces warm neutral atomic gas, rather than recombination emission from ionized and cooling post-shock gas. Although Mg II line intensity ratios, line profiles, and radial velocities in spectra will be helpful to confirm this, our conjecture of resonant scattering based on images alone relies upon 3 key observed properties:

1. The structures immediately outside the Homunculus are unique to images in the F280N filter; these structures are not seen in any other continuum or emission line images of η Car that we are aware of. Since they are not seen in the adjacent broad F336W filter, they are not due to UV

continuum scattered light and must be Mg II line emission. However, gas that emits Mg II through recombination or collisional excitation because it is photoionized or shock excited would also be seen in other emission-line diagnostics like H α , [N II], or [Fe II]. Resonant scattering is a mechanism to preferentially cause Mg II emission.

2. The morphology of the F280N features shows radial streaks and a smoother overall distribution than other line-emitting features in the Outer Ejecta. Long, smooth, radial streaks may arise naturally if they are tracing beams of scattered starlight escaping through holes and cracks with low optical depth, in between dust clumps. Indeed, the polar lobes of the Homunculus present a complicated network of dust clumps and filaments (Morse et al. 1998). Shadows cast by these clumps contribute to the contrast of the streaks, with dark lanes projecting out radially. Similarly, long wavelength imaging of the equatorial belt inside the Homunculus reveals a clumpy, disrupted torus with holes through which starlight can escape (Chesneau et al. 2005; Smith et al. 2002, 2018c, 2003b). This may help account for the prominent radial streaks that connect the Homunculus equatorial skirt to shocked clumps in the NN Jet and S Con-

densation. However, since these radial streaks are absent, less prominent, or have different intensity distributions in continuum images, they cannot be due to dust scattering. Line resonance scattering is needed. In stark contrast, emission features in the Outer Ejecta seen in other lines like [N II] and [Fe II] — which *are* expected to trace post-shock cooling emission — do not show a smooth and radially streaked morphology. Instead, these lines trace a highly complex network of small-scale clumps and filaments that might arise naturally from rapid radiative cooling in dense post-shock gas.

3. The location of the most prominent F280N emission appears as a diffuse halo sandwiched in between a thin shell of cold, dense, molecular gas and dust in the Homunculus (Smith 2002a, 2006; Smith et al. 2003b) at its inner boundary, and the shell of hot, shock-ionized outer ejecta (Walborn 1976; Davidson et al. 1982; Smith & Morse 2004; Weis et al. 1999, 2001) at its outer boundary. This is an intermediate ionization transition zone where one might naturally expect to find warm and predominantly neutral atomic gas, well-suited to produce Mg II resonance scattering if it is bathed in non-ionizing radiation. Indeed, this region is exposed to strong near-UV Balmer continuum (non-ionizing radiation) from η Car at locations where starlight can escape through cracks in the clumpy Homunculus. This is non-ionizing Balmer continuum starlight that escapes, because essentially all the Lyman continuum is choked off at much smaller radii by η Car’s extremely dense stellar wind (Hillier et al. 2006; Smith et al. 2003a). This escaping near-UV starlight can ionize Mg⁰ to Mg⁺ (7.6 eV), but because there are no Lyman continuum photons, it cannot ionize the gas to Mg⁺⁺ (requiring 15 eV). This makes it highly probable that near-UV starlight escaping through holes in the Homunculus will encounter Mg⁺ atoms in the ground state, and emit the streaked Mg II $\lambda\lambda 2796, 2803$ that we see.

The Mg II $\lambda\lambda 2796, 2803$ resonant doublet ($3s^2S-3p^2P^0$) is magnesium’s analog of the Ca II HK lines. Ca II HK emission may be weaker or absent in this same region, however, because of the lower Ca abundance (relative to Mg) at solar metallicity, and because Ca⁺ can be ionized to Ca⁺⁺ by near-UV photons above 11.8 eV but below 13.6 eV, which may escape η Car’s stellar wind and the Homunculus. It is interesting to note, however, that Ca II HK has been detected in long-slit spectra, but seen in *absorption* arising from a thin shell of neutral gas immediately outside the SE polar lobe of the Homunculus (Davidson et al. 2001; Smith 2002a). This Ca II structure in absorption is not the same as the Mg II emission structures discussed here, but it may be related (see Section 4.3 below).

Generally, Mg II emission is seen in all directions immediately outside the Homunculus and inside the N-rich shell that includes the S Ridge, S Condensation, and NN Jet, but the Mg II emission is brightest over the poles, while the spikes are most dramatic in the equatorial skirt. Regions with strong Mg II emission also tend to be locations where [N II] emission is relatively weak. Some of the detailed Mg II features are discussed below.

4.2 Structure of Mg II over the poles and the Ghost Shell

Much of the F280N flux is concentrated in dramatic radial structures in the gas beyond the edges of the bipolar Homunculus lobes (Figure 5). The Mg II emission just outside the SE (approaching) lobe bears the hallmarks of so-called “God rays” — such as seen at the edges of terrestrial clouds or mountains — due to shadows cast by opaque dust features on the lobe surface. This important phenomenon seems to isolate soft UV emission from the central star as the source of exciting resonantly scattered photons (see above). The Mg II emission structures outside the NW (receding) lobe may also result from opaque dust features on that lobe, though the morphology is more filamentary, reminiscent of the spiked hair of a troll doll.

A second interesting feature is the dark rim right at the edge of the SE lobe where there is a $\sim 0.5''$ -wide deficit of Mg II emission. There may be an isolated example of a similar dark edge at one position at the bottom of the NW lobe, but in general there is no similarly prevalent dark feature around the edge of the NW lobe. The origin of this dark edge of the SE lobe and the general lack of a similar feature at the edge of the NW lobe is unclear. One possibility is that it is either a shadow or absorption caused by high optical depths at the limb-darkened edge of a thin and dense gas shell immediately outside the Homunculus lobes. Alternatively, Mg II emission could be absent at this location, in principle, because Mg atoms in a thin layer on a skin outside the Homunculus lobes are either predominantly ionized to Mg⁺⁺ or have recombined to be mostly neutral Mg⁰.

Although the specific features traced by Mg II emission outside the polar lobes have not been seen in any previous imaging of η Car, some observations have suggested the existence of a possibly related polar shell or bubble outside the SE polar lobe. Optical and IR long-slit spectra have revealed blueshifted absorption from a thin (unresolved velocity width much less than the expansion speed of several hundred km s⁻¹) polar structure outside the Homunculus SE polar lobe seen in Ca II HK absorption and He I $\lambda 10830$ absorption (Davidson et al. 2001; Smith 2002a), as well as narrow H α and [N II] emission (Currie et al. 2002; Smith et al. 2003a; Mehner et al. 2016) and near-IR [Fe II] emission (Smith 2002a, 2006). As noted in the Introduction, Currie et al. (2002) referred to this structure as the “Ghost shell”. This structure does not appear to extend spatially beyond the border of the SE lobe, and its velocity structure suggests that it is a thin bubble. It is therefore not coincident with the Mg II emission structures that are seen to extend more than $5''$ outside the polar lobes in images, and cover a wide range of radii (thus suggesting a range of expansion speeds in a Hubble-like flow). Nevertheless, both structures are outside the SE polar lobe and inside the radius of the ragged [N II]-emitting shell seen as the S Ridge and S condensation, so they may be physically related. Based on its velocity structure and spatial location, the Ghost Shell appears to be limited to a smaller range of radii at the outer boundary of the SE polar lobe, perhaps related to the dark edge of the SE lobe seen in Mg II. Long-slit UV spectra of this faint Mg II emission outside the polar lobes are needed to further investigate its velocity structure and possible kinematic relationship to the Ghost Shell.

4.3 Equatorial Mg II Emission

Another dramatic feature seen in Mg II emission is the revelation of complete, possibly organized, jet-like features in the equatorial debris. The NN Jet has long been interpreted as a fast-moving column of material with an associated bow shock (e.g., Meaburn et al. 1993). Its core structure appears somewhat disembodied at its base in [N II] F658N images, and even more ragged in F336W and other continuum-dominated images. However, the Mg II emission from the NN Jet core is brightest at the base and can be traced all the way back to the Homunculus equatorial region as a smooth and contiguous beam of UV light.

Likewise, the S Condensation on the opposite side of the Homunculus from the NN Jet has long been recognized as a shock interface between fast ejecta and circumstellar material (Dufour et al. 1999). While there were faint indications of connected material in the [N II] and blue continuum images back toward the central star (Morse et al. 1998), the Mg II emission again shows a bright, contiguous column of material connecting the outer portions of the S Condensation all the way back to the Homunculus equatorial skirt. Moreover, there is another well-defined thin column of light just south of the S Condensation column, rotated by $\sim 15^\circ$. These two radial beams of UV light seem to outline a dense clump of shadowing dust in the equatorial skirt, located $4''$ west and $2''$ south of the central star.

Thus the Mg II data show emphatically that the NN Jet and S Condensation are the same phenomenon, characterized observationally by a contiguous beam of resonantly scattered Mg II emission connecting to fast-moving, shocked condensations in the Outer Ejecta. These appear to be very special directions in the equatorial plane.

Do these radial UV beams appear because that is where dense material lies in the outer parts of an equatorial skirt, or do we see them because they are akin to searchlights, extending from a hole at smaller radii where UV light escapes? Their smooth and perfectly radial structure seems to imply the latter, as with the streaked Mg II emission over the polar lobe regions outside the Homunculus. On the other hand, there are indeed dense, shocked gas structures at the terminus of each of the beams of UV light, and the NN Jet even includes a well-defined bow-shock structure that surrounds the end of that UV beam. The clumpy, dense [N II]-emitting structure in the same directions indicate that there is indeed a dense outflow of fast-moving material here. Taken together, the fast, shocked [N II]-emitting knots in the S Condensation and NN jet, and the Mg II beams, may suggest that dense knots of fast-moving gas blasted through the equatorial torus in these directions, leaving a tunnel in their wake through which radial beams of near-UV light can now escape. The escaping beams of UV light require that whatever may have punched these holes in the equatorial torus, the prominent holes in these special directions have persisted since the Great Eruption.

In fact, the dense equatorial waist of the Homunculus is seen at long mid-IR to submm wavelengths to be a disrupted and clumpy toroidal structure (Chesneau et al. 2005; Smith et al. 2002; Smith 2005; Smith et al. 2018c), making it likely that UV starlight is blocked in most azimuthal directions, but may escape between clumps in certain preferred directions. The current surviving companion to η Car is on

a very eccentric orbit with a known orientation in 3-D space (Madura et al. 2012). Interestingly, it has been noted that these two directions of the S Condensation and NN Jet, respectively, correspond to directions where this companion star might have plunged into and out of a disk around the erupting star (Smith et al. 2018b,c), if such a disk were responsible for pinching the waist of the Homunculus during the Great Eruption.

We note that there is also faint, diffuse Mg II emission located outside the Homunculus at locations that seem to coincide with latitudes within very roughly $\pm 45^\circ$ above and below the equatorial plane, corresponding to mid-latitudes of the Homunculus. As with the Mg II in the polar directions, this diffuse emission is bounded at its inner edge by the Homunculus and bounded on its outer edge by the bright [N II] shell. It is, however, much fainter than the emission near the polar axes.

4.4 Mg II emission, shocked [N II] emission, and X-rays

Figure 6 shows the same 3-color *HST* image from Figure 2, but superposed upon the extended X-ray emission from η Car detected by the *Chandra X-ray Observatory*, with the X-ray emission shown in purple. Although this image includes 0.5-7 keV flux, most of the extended X-ray emission is concentrated in the softer X-ray band at 0.5-1 keV (Seward et al. 2001; Corcoran et al. 2004; Hamaguchi et al. 2014).

The main shell of extended X-ray emission marks a shock front between the fastest N-rich ejecta and an ancient pre-eruption wind. N abundances are higher inside X-ray shell and lower outside it (Smith & Morse 2004). Moreover, the fastest Doppler shifts in the Outer Ejecta are seen from diffuse N-rich filaments inside the soft X-ray shell that can only be detected in spectra (Smith 2008), whereas the dense knots and clumps seen in F658N images with *HST* are slower (Mehner et al. 2016; Weis et al. 2001, 1999) and arise from eruptions 300 or 600 years before the Great Eruption (Kiminki et al. 2016). This suggests that the main soft X-ray shell is truly a blast wave from the Great Eruption, making the shocked shells surrounding η Car somewhat analogous to a low-energy SNR. The kinematics and geometry of the Outer Ejecta are complicated, originating from a series of previous eruptions. Kiminki et al. (2016) and Mehner et al. (2016) have recently discussed the structure and kinematics of the Outer Ejecta in detail.

Since the main X-ray shell seen at relatively large radii is now crashing into ejecta from previous eruptions, one can assume that it has largely cleared away the older material that may have been located closer to the star in the past. The vast majority of ejecta inside the X-ray shell was ejected more recently, either during the main event of the 19th century Great Eruption (Smith 2017; Morse et al. 2001), in the decades leading up to that eruption (Kiminki et al. 2016), or minor eruptions afterward (Smith et al. 2004a; Dorland et al. 2004). As noted earlier, the Mg II-emitting structures discovered here are sandwiched in between the Homunculus (with a well-determined ejection date of 1847) and the bright [N II]-emitting Outer Ejecta in the S Ridge and similar features, which have dates of origin from proper motions that are either associated with the Great Eruption

or within decades before the 1840s (Kiminki et al. 2016). Moreover, there is a clear deficit of X-ray emission at the locations of the brightest Mg II, emission itself, indicating that there is not a strong gradient in the velocity or characteristic age of material at this position (i.e., the Mg II emission arises from gas in free expansion, and does not arise at a shock interface where fast young material collides with slower older material). We therefore conclude that the Mg II-emitting structures were most-likely ejected by the star either in the main event of the Great Eruption, or perhaps in the decades leading up to it. If so, its expansion speed away from the star should be similar to or somewhat faster than the expansion of the polar lobes of the Homunculus (Smith 2006), moving at 650 km s^{-1} . This would suggest that the Mg II structures are moving at roughly $700\text{--}1000 \text{ km s}^{-1}$ based on their location. Proper motions from a second epoch of F280N imaging and/or Doppler velocities from Mg II $\lambda 2800$ spectra are needed to more tightly constrain the speed and time of origin of the Mg II, features. The kinematics of this material could be of great interest if Mg II structures probe the polar mass-loss of η Car in the decades leading up to the Great Eruption. This may offer an important diagnostic of the star system's growing instability, especially in the context of a possible merger event (Smith et al. 2018b; Portegies Zwart & van den Heuvel 2016).

4.5 Another connection to SLSNe

The violent, impulsive mass ejection exemplified by η Carinae in its 19th century eruption has been compared to the extreme pre-SN mass-loss of some SNe that show signatures of very strong shock interaction with circumstellar material, including SNe of Types IIn and Ibn (see Smith 2014). Most notable among these are the cases of several super-luminous SNe of Type IIn, such as the well studied cases of SN 2006gy and SN 2005tf (Smith et al. 2007, 2008). The physical parameters of their impulsive pre-SN mass loss events include massive shells ($\sim 20 M_{\odot}$) ejected at speeds of hundreds of km s^{-1} , for which the only known precedent in nearby stellar populations is the Great Eruption of η Car.

In a recent study of the Type Ic super-luminous supernova iPTF16eh, Lunnan et al. (2018) discovered an unusual Mg II resonance light echo associated with the event. From the evolution of this Mg II echo, those authors inferred the existence of a massive, detached (0.1 pc) circumstellar shell ejected in an impulsive mass-loss event decades before the SN. Interestingly, they drew some comparisons to the nebula around η Carinae, although there are differences as well (for instance, those authors infer a spherical geometry for the shell, unlike the bipolar ejecta around η Car). Spectra of iPTF16eh indicated that the SN photosphere itself was hydrogen poor (Lunnan et al. 2018), but the H abundance in the detached shell is not yet known because so far it is only seen in resonance scattering of Mg II; its composition might be constrained by forthcoming observations obtained if/when the fast SN ejecta overtake and shock the detached shell. Although we would not necessarily expect the Mg II-emitting structures around η Car to maintain the same level of ionization if η Car were to explode as a super-luminous SN, we nevertheless found it noteworthy that both η Car and an SLSN have dense shells seen in the unique tracer of near-UV Mg II resonant scattering.

4.6 Mass of unshocked, neutral gas from Mg II emission

Since the structures seen here for the first time in resonant scattering of Mg II $\lambda 2800$ are not seen in any other previous imaging of η Car, and are presumably dominated by neutral atomic gas, we cannot estimate their mass via normal diagnostics like thermal-IR dust emission or molecular emission, nor via recombination or collisionally excited emission from ionized plasma. We can, however, make a crude guess at the gas mass based on the Mg II emission itself and the assumption of resonant scattering. Future spectroscopy of the Mg II doublet can constrain the line scattering optical depth as well as the true expansion velocity of the gas. But for now we can make the rough assumption that for resonant scattering to be efficient, the optical depth of the brighter line at 2796 \AA is probably close to unity, i.e., $\tau_{2796} \approx 1$. Following Martin et al. (2013), who made a similar assumption in an analysis of the Mg II scattering halos of galaxies, the Sobolev optical depth can be written as

$$\tau_{2796} = 4.6 \times 10^{-7} \text{ cm}^3 \text{ s}^{-1} n_{Mg^+} \left(\frac{dv}{dr} \right)^{-1} \quad (1)$$

where dv/dr is the velocity gradient at the location where the line scattering optical depth reaches unity, and which we assume is constant in this case with a Hubble-like flow. Adopting representative values of $v=700 \text{ km s}^{-1}$ for the expansion speed and $r=22,000 \text{ AU}$ for the outer radius of the polar lobes of the Homunculus (Smith 2006), and setting $\tau_{2796}=1$, we have

$$n_{Mg^+} \simeq 5 \times 10^{-4} \text{ cm}^{-3} \left(\frac{v}{700 \text{ km s}^{-1}} \right) \left(\frac{r}{22,000 \text{ AU}} \right)^{-1} \quad (2)$$

for the number density of Mg II scattering atoms, which may be a conservative lower limit if there is additional mass hidden in very optically thick clumps. To convert this to a total H gas density, we need to correct for the abundance of Mg, n_{Mg}/n_H , the ionization fraction of Mg, $\chi = n_{Mg^+}/n_{Mg}$, and the fraction of the total Mg atoms that are left in the gas phase and not depleted onto dust grains, $f_g = n_{Mg}(\text{gas}) / n_{Mg}(\text{total})$, i.e.,

$$n_H = n_{Mg^+} \left(\frac{n_{Mg}}{n_H} \chi f_g \right)^{-1}. \quad (3)$$

To be conservative, we adopt $\chi=1$, although some fraction of the Mg may be Mg^0 or Mg^{++} . We assume a solar abundance of Mg, roughly $n_{Mg}/n_H = 4 \times 10^{-5}$. Unfortunately, for the goal of using Mg emission to constrain the mass, the large condensation temperature of Mg around 1300 K means that a large fraction of Mg atoms are typically depleted onto dust grains (leaving a small value of f_g for Mg atoms in the gas phase), requiring a large and uncertain correction factor. From studies of the warm and cool atomic gas in the Galactic ISM, Savage & Sembach (1996) estimate values for Mg in the gas phase of roughly 3% to 13%. Adopting the larger gas fraction for a conservative estimate, we therefore find an approximate density of $n_H \approx 100 \text{ cm}^{-3}$. This may be an underestimate if there are clumps with high optical depth, or if more significant Mg depletion onto grains leaves a lower atomic gas fraction of Mg.

To estimate the total mass of the Mg II resonance scattering shell around η Car, we have $M = m_H n_H V$, where $V = (4/3)\pi(R_{out}^3 - R_{in}^3)$ is the volume of a hollow spherical shell. Taking $R_{in}=22,000$ AU as the inner radius (matching the outer extent of the Homunculus lobes at the pole; Smith 2006) and $R_{out}=30,000$ AU as an approximate outer radius, the derived H density would imply a total mass of roughly 4×10^{31} g or about $0.02 M_\odot$. Expanding with a typical speed of around 800 km s^{-1} , this mass has a total kinetic energy of around 1.3×10^{47} erg. We caution that these are very rough, order of magnitude estimates, although we also noted reasons why they may be conservative underestimates if wrong. These values are very small compared to the total mass and kinetic energy budget of the Great Eruption of around $15 M_\odot$ and 10^{50} erg (Smith et al. 2003a; Smith 2006, 2008). They are comparable, however, to values estimated for the mass loss of the 1890 Lesser Eruption, which was roughly $0.1 M_\odot$ and $10^{46.9}$ erg (Smith 2005; Ishibashi et al. 2003).

Putting these mass and kinetic energy estimates in context requires more information about the origin of the gas in the Mg II scattering halo. Proper motions and radial-velocity structure in long-slit spectra are needed for this. Residing outside the Homunculus polar lobes, it is interesting to speculate that this material might provide some clues about the mass-loss and instability of the star in the decades leading up to the peak of the Great Eruption. Spectroscopy of light echoes (Rest et al. 2012; Prieto et al. 2014; Smith et al. 2018a,b) shows relatively low outflow speeds of $150\text{--}200 \text{ km s}^{-1}$ in the early phases of the eruption. However, these echoes view η Car from a vantage point near the equatorial plane. If there was a dense and slow equatorial outflow in early phases, as expected in the scenario of a binary merger (Smith et al. 2018b), this slow and dense outflow would likely dominate spectra, but does not preclude a somewhat less dense and faster wind in the polar direction. A polar wind might be expected if the pre-eruption star was rapidly rotating (Owocki et al. 1996; Owocki & Gayley 1997; Owocki et al. 1998; Dwarkadas & Owocki 2002). The Mg II-emitting gas reported here may therefore provide important and unique clues about η Car’s early mass loss and instability. Alternatively, the Mg II-emitting gas may have some other origin, such as material that leaked through the clumpy polar lobes due to hydrodynamic instabilities.

5 SUMMARY

We present the first *HST*/WFC3 UVIS and IR images of η Carinae. The most significant new result is that a deep image in the F280N filter, never used before to image η Carinae, shows extended nebular structures outside the bipolar Homunculus nebula that have not been visible in any previous continuum or emission-line images. The F280N filter includes Mg II $\lambda\lambda 2796, 2803$ emission that traces low-ionization atomic gas (mostly neutral H, low ionization metals). It arises from a transition zone that appeared as a void in previous images, coming from an apparent cavity outside the molecular Homunculus polar lobes, but inside the shock-ionized Outer Ejecta. We note a very striking radially streaked morphology to the Mg II emission, and we suspect that these arise from radial beams of UV light escaping the clumpy Homunculus. In some cases, dark spaces between

these radial streaks connect back to dense dust clumps in the polar lobes or equatorial skirt, as if they are long shadows projecting out into the regions outside the Homunculus.

While neutral atomic gas is hard to detect because it is invisible in most tracers, it may show up well in resonance scattering lines near a strong light source. This fact, plus the observed Mg II morphology (including pronounced radial streaks) and an anticorrelation with emission from shocked clumps, leads us to propose that resonance scattering is the dominant emission mechanism giving rise to the F280N emission outside the Homunculus that we detect. We derive a mass of around $0.02 M_\odot$ or more, and an outflow kinetic energy around 10^{47} erg for the gas traced by Mg II. This is small compared to the total mass and energy budget of the Great Eruption, although this estimate required assumptions that were chosen to be on the conservative side. Thus, the quoted mass and energy might be underestimates, perhaps by as much as an order of magnitude. Nevertheless, the Mg II emission may be tracing a component of the outflow that provides important clues to the early phases of the Great Eruption before the main Homunculus polar lobes were ejected, thus providing information about the building instability of the star. These mass and energy estimates, and constraints on the date of origin for the material, can be improved with future *HST* spectroscopy and proper motions of the Mg II emission.

To our knowledge, no other LBVs have been observed with deep F280N imaging, so we do not know if the Mg II nebula around η Carinae is unique. We suspect, though, that resonance scattering of Mg II might be a good tracer of neutral or low-ionization gas in a variety of stellar outflows where warm gas is bathed in near-UV light, but where the central star might not be hot enough to fully ionize the outflow or not cool enough (or the outflow is not dense enough) to allow all the CSM to condense into dust and molecules. One example already mentioned is the case of a Mg II resonance scattering nebula around a distant super-luminous SN (Lunnan et al. 2018). Another example is the outflows from protostellar objects, where a shock-ionized component of the outflow is seen in visible-wavelength emission lines as Herbig-Haro (HH) jets, and where molecular outflows are seen at IR and radio wavelengths. Comparing the two, molecular envelopes generally show a substantial excess of momentum as compared to the ionized gas in the collimated jets or bow shocks (e.g. Dionatos & Güdel 2016), suggesting a low ionization fraction in the jet outflow and a larger reservoir of atomic gas. Indeed, comparing $H\alpha$ to tracers of low-ionization gas reveals that the ionized gas emitting $H\alpha$ can be only a small portion of the jet outflow (Reiter et al. 2015, 2017). Perhaps Mg II resonance scattering would be a useful way to trace this low ionization gas in cases that do not suffer too much foreground extinction.

ACKNOWLEDGEMENTS

We acknowledge helpful comments from the referee, which helped to clarify several aspects of the observations and analysis presented in this paper. We thank STScI science and technical staff members Peter McCullough and Amber Armstrong for special assistance in planning the DD time observations and Joe DePasquale for producing the color *HST* image in Figure 2 and the similar image superposed on the *Chandra* X-ray image in Figure 6. We thank both Kenji Hamaguchi and Mike Corcoran for discussions over many years concerning the X-ray emission from η Car’s outer shell. JM appreciates helpful discussions with John Raymond and Pat Hartigan.

Based on observations made with the NASA/ESA Hubble Space Telescope, obtained at the Space Telescope Science Institute, operated by the Association of Universities for Research in Astronomy, Inc., under NASA contract NAS 5-26555. Support was provided by NASA through grants GO-15596, GO-15289, GO-14768, and AR-14586 from the Space Telescope Science Institute, which is operated by the Association of Universities for Research in Astronomy, Inc., under NASA contract NAS 5-26555. NS's research on Eta Carinae also received support from NSF grants AST-1312221 and AST-1515559.

REFERENCES

- Aghakhanloo M, Murphy J, Smith N, Hlozek R. 2017, *MNRAS*, 472, 591
- Blair WP, Morse JA, Raymond JC, Kirshner RP, Hughes JP, Dopita MA, Sutherland RS, Long KS, Winkler PF. 2000, *ApJ*, 537, 667
- Chesneau O. et al. 2005, *A&A*, 435, 104
- Chevalier, R.A., Kirshner, R.P. 1978, *ApJ*, 219, 931
- Chevalier, R.A., Liang, E.P. 1989, *ApJ*, 344, 332
- Corcoran, M. F., Hamaguchi, K., Gull, T., et al. 2004, *ApJ*, 613, 381
- Currie, D. G., et al. 1996, *AJ*, 112, 1115
- Currie, D. G., et al. 2002 - ghost shell
- Damineli, A. 1996, *ApJ*, 460, L49
- Davidson K., Walborn N. R., Gull T. R., 1982, *ApJ*, 254, L47
- Davidson, K., Smith, N., Gull, T. R., Ishibashi, K., & Hillier, D. J. 2001, *AJ*, 121, 1569
- Dionatos O., Güdel M., 2016, *A&A*, 597, A64
- Dorland, B. N., Currie, D. G., & Hajian, A. R. 2004, *AJ*, 127, 1052
- Dufour RJ, Glover TW, Hester JJ, Currie DG, van Orsow D, Walter DK. 1999, in *ASP Conf. Ser.* 179, *Eta Carinae At The Millennium*, ed. JA Morse et al. (San Francisco: ASP), 134
- Dwarkadas VV, Owocki SP. 2002, *ApJ*, 581, 1337
- Gaviola, E. 1950, *ApJ*, 111, 408
- Gull TR, Viera G, Bruhweiler F, Nielsen KE, Verner E, Danks A. 2005, *ApJ*, 620, 442
- Gull TR, Kober GV, Nielsen KE. 2006, *ApJS*, 163, 173
- Hamaguchi K., Corcoran M. F., Russell C. M. P. et al., 2014, *ApJ*, 784, 125
- Hartigan, P., Raymond, J., Hartmann, L. 1987, *ApJ*, 316, 323
- Hartigan, P., Raymond, J., Pierson, R. 2004, *ApJ*, 614, L69
- Herschel J.F.W. 1847, *Results of Astronomical Observations Made during the Years 1834, 5, 6, 7, 8 at the Cape of Good Hope* (London: Smith, Elder & Co.)
- Hester JJ, Light RM, Westphal JA, Currie G, Groth EJ, Holtzmann JA, Lauer TR, O'Neil EJ. 1991, *AJ*, 102, 654
- Hillier, D. J., & Allen, D. A. 1992, *A&A*, 262, 153
- Hillier, D. J., Gull, T., Nielsen, K., et al. 2006, *ApJ*, 642, 1098
- Ishibashi K. et al., 2003, *AJ*, 125, 3222
- Kiminki MM, Reiter M, Smith N. 2016, *MNRAS*, 463, 845
- Lunnan R, Fransson C, Vreeswijk PM, et al. 2018, *Nature Astronomy*, 2, 887
- Madura T.I., et al. 2012, *MNRAS*, 420, 2064
- Martin CL, Shapley AE, Coil AL, Kornei KA, Murray N, Pancoast A. 2013, *ApJ*, 770, 41
- Meaburn, J., Gehring, G., Walsh, J.R., Palmer, J.W., Lopez, J.A., Bryce, M., Raga, A.C. 1993, *A&A*, 276, L21
- Mehner A, et al. 2016, *A&A*, 595, A120
- Morse, J. A., Davidson, K., Bally, J., Ebbets, D., Balick, B., Frank, A. 1998, *AJ*, 116, 2443
- Morse J. A., Kellogg J. R., Bally J., Davidson K., Balick B., Ebbets D., 2001, *ApJ*, 548, L207
- Nielsen K. E., Gull T. R., Viera Kober G., 2005, *ApJS*, 157, 138
- Owocki SP, Gayley KG. 1997, in *Luminous Blue Variables: Massive Stars in Transition*, *ASP Conf. Ser.* 120, ed. A. Nota & H. Lamers (San Francisco: ASP), 121
- Owocki SP, Cranmer SR, Gayley KG. 1996, *ApJ*, 472, L115
- Owocki SP, Gayley KG, Cranmer SR. 1998, in *ASP Conf. Ser.* 131, *Boulder Munich II: Properties of Hot Luminous Stars*, ed. I. D. Howarth (San Francisco: ASP), 237
- Owocki S. P., Gayley K. G., Shaviv N. J., 2004, *ApJ*, 616, 525
- Portegies Zwart S. F., van den Heuvel E. P. J., 2016, *MNRAS*, 456, 3401
- Prieto JL, et al. 2014, *ApJ*, 787, 8
- Reiter M, Smith N, Kiminki MM, Bally J. 2015, *MNRAS*, 450, 564
- Reiter M, Kiminki MM, Smith N, Bally J. 2017, *MNRAS*, 470, 4671
- Rest A, et al. 2012, *Nature*, 482, 375
- Savage B, Sembach K. 1996, *ARA&A*, 34, 279
- Seward, F. D., Butt, Y. M., Karovska, M., Prestwich, A., Schlegel, E. M., Corcoran, M. F. 2001, *ApJ*, 553, 832
- Shaviv NJ. 2000, *ApJ Letters*, 532, L137
- Smith N. 2002a, *MNRAS*, 337, 1252
- Smith N. 2002b, *MNRAS*, 336, L223
- Smith N. 2004, *MNRAS*, 351, L15
- Smith N. 2005, *MNRAS*, 357, 1330
- Smith N. 2006, *MNRAS*, 644, 1151
- Smith N. 2008, *Nature*, 455, 201
- Smith N. 2013, *MNRAS*, 429, 2366
- Smith N. 2014, *ARAA*, 52, 487
- Smith N. 2017, *MNRAS*, 471, 4465
- Smith N., Davidson K., 2001, *ApJ*, 551, L101
- Smith N., Ferland G. J., 2007, *ApJ*, 655, 911
- Smith N, Frew D. 2011, *MNRAS*, 415, 2009
- Smith N, Hartigan P. 2006, *ApJ*, 638, 1045
- Smith N, Morse JA. 2004, *ApJ*, 605, 854
- Smith N, Owocki SP, 2006, *ApJ*, 645, L45
- Smith N, Tombleson R. 2015, *MNRAS*, 447, 602
- Smith, N., Morse, J. A., Davidson, K., Humphreys, R. M. 2000, *AJ*, 120, 920 L145
- Smith N., Gehrz R. D., Hinz P. M., Hoffmann W. F., Mamajek E. E., Meyer M. R., Hora J. L. 2002, *ApJ*, 567, L77
- Smith N, Davidson K, Gull TR, Ishibashi K, Hillier DJ. 2003a, *ApJ*, 586, 432
- Smith N., Gehrz R. D., Hinz P. M., Hoffmann W. F., Hora J. L., Mamajek E. E., Meyer M. R., 2003b, *AJ*, 125, 1458
- Smith N., Morse, J.A., Gull T.R., et al., 2004a, *ApJ*, 605, 405
- Smith N., Morse J. A., Collins N. R., Gull T. R., 2004b, *ApJ*, 610, L105
- Smith N., Li W., Foley RJ, et al. 2007, *ApJ*, 666, 1116
- Smith N., Chornock R., Li W., et al. 2007, *ApJ*, 686, 467
- Smith N., et al. 2011, *MNRAS*, 415, 773
- Smith N, Rest A, Andrews JE, Matheson T, Bianco FB, Prieto JL, James DJ, Smith RC, Strampelli GM, Zenteno A. 2018a, *MNRAS*, 480, 1457
- Smith N, Andrews JE, Rest A, Bianco FB, Prieto JL, Matheson T, James DJ, Smith RC, Strampelli GM, Zenteno A. 2018b, *MNRAS*, 480, 1466
- Smith N., Ginsburg A, Bally J. 2018, *MNRAS*, 474, 4988
- Steffen W, Teodoro M, Madura TI, et al. 2014, *MNRAS*, 442, 3316
- Sutherland RS, Dopita MA. 1995, *ApJ*, 439, 381
- Teodoro M., Damineli A., Sharp R. G., Groh J. H., Barbosa C. L., 2008, *MNRAS*, 387, 564
- Van Dyk SD, Matheson T. 2012, in *Eta Carinae and the Supernova Impostors*, ed. R.M. Humphreys and K. Davidson (Springer)
- van Marle AJ, Owocki SP, Shaviv NJ. 2008, *MNRAS*, 389, 1353
- van Marle AJ, Owocki SP, Shaviv NJ. 2009, *MNRAS*, 394, 595
- Verner E., Bruhweiler F., Nielsen K. E., Gull T. R., Viera kober G., Corcoran M. F., 2005, *ApJ*, 629, 1034
- Walborn N. R., 1976, *ApJ*, 204, L17

- Walborn, N. R., Blanco, B. M., Thackeray, A. D. 1978, ApJ, 219, 498
- Weigelt G, Kraus S. 2012, ASSL, 384, 129
- Weis K., 2012, in Davidson K., Humphreys R. M., eds, Astrophysics and Space Science Library, Vol. 384. Astrophysics and Space Science Library. p. 171
- Weis K., Duschl W. J., Chu Y.H. 1999, A&A, 349, 467
- Weis K., Duschl W. J., Bomans D. J., 2001, A&A, 367, 566
- Woosley SE. 2017, ApJ, 836, 244